

Optimal trajectories for Bayesian olfactory search in turbulent flows: the low information limit and beyond

R. A. Heinonen,¹ L. Biferale,¹ A. Celani,² and M. Vergassola³

¹*Dept. Physics and INFN, University of Rome “Tor Vergata”,
Via della Ricerca Scientifica 1, 00133 Rome, Italy*

²*Quantitative Life Sciences, The Abdus Salam International Centre for Theoretical Physics, 34151 Trieste, Italy*

³*Laboratoire de physique, École Normale Supérieure, CNRS,
PSL Research University, Sorbonne University, Paris 75005, France*

In turbulent flows, tracking the source of a passive scalar cue requires exploiting the limited information that can be gleaned from rare, stochastic encounters with the cue. When crafting a search policy, the most challenging and important decision is what to do in the absence of an encounter. In this work, we perform high-fidelity direct numerical simulations of a turbulent flow with a stationary source of tracer particles, and obtain quasi-optimal policies (in the sense of minimal average search time) with respect to the empirical encounter statistics. We study the trajectories under such policies and compare the results to those of the infotaxis heuristic. In the presence of a strong mean wind, the optimal motion in the absence of an encounter is zigzagging (akin to the well-known insect behavior “casting”) followed by a return to the starting location. The zigzag motion generates characteristic $t^{1/2}$ scaling of the rms displacement envelope. By passing to the limit where the probability of detection vanishes, we connect these results to the classical linear search problem and derive an estimate of the tail of the arrival time pdf as a stretched exponential, which agrees with Monte Carlo results. We also discuss what happens as the wind speed decreases.

INTRODUCTION. A wide variety of animals, from plankton [1] to fruit flies [2] to dogs [3], combine olfactory sensing of odors with complex search behaviors which enable them to track the sources of the odors [4]. A famous, striking example is the ability of moths to locate, starting from $\gtrsim 100$ m away, potential mates using a single sex pheromone cue to which they are sensitive via olfactory organs [5–7]. In many settings, including those relevant to flying insects [8], this olfactory search behavior occurs in a fully turbulent flow. Turbulent conditions are also relevant to chemical-sensing robots, which may be used to locate hazardous substances, fires or explosive devices [9–12].

The consequences of turbulence in the olfactory search problem, by now well-studied [4, 13–15], cannot be overstated. Odors may be modeled as passive scalars; the turbulent transport of passive scalars exhibits a remarkable degree of spatiotemporal intermittency, and the concentration fluctuations exhibit strongly non-Gaussian statistics [16]. As odors are emitted by a stationary and continuous source and mix into the surrounding flow, they form a characteristic concentration profile called a plume, whose shape depends on details of the flow. Within the plume, the concentration fluctuates wildly on account of the turbulence, forming a complex and patchy landscape (see Fig. 1 for a visualization from simulation). If a searcher is sensitive to an odor above some detection threshold, its encounters with the odor are randomized and typically rare (except when the searcher is close to the source) [15]. Moreover, the odor typically manifests in isolated patches rather than a continuous field, rendering simple gradient-based search strategies effectively useless.

How should a searcher respond to these limited, random encounters in order to locate the source in minimal

average time? Looking to biology can provide some inspiration. During upwind flight, a diverse array of flying insects exhibit a behavior called “casting,” which consists of broad zigzags perpendicular to the wind direction. Wind tunnel experiments suggest that this behavior is a very generic response to loss of contact with the odor cue [17, 18]. [In biological literature, “zigzagging” often refers to a specific insect behavior consisting of small-scale crosswind motion combined with upwind flight. We will frequently use the word “zigzagging” as simply a qualitative description of trajectories, without intending reference to this behavior.]

For robotics applications, this observation may be used to formulate biomimetic strategies, as in [14]. Alternatively, if the searcher is equipped with a model for the spatially-dependent likelihood of an encounter, the search problem may be formalized as a Bayesian partially-observable Markov decision process (POMDP) [19]. This formulation allows the *optimal*, i.e., minimum average time, search strategy to be described by a dynamic programming (Bellman) equation, which may be approximately solved [20–22].

The model likelihood is the key physics input into the problem. Previous work on the POMDP approach imposed a model likelihood *ad hoc*, with the effects of turbulence captured by an effective diffusivity only. The realism of such a model is highly dubious in light of the complexity of turbulent transport; it is certain to fail, for example, in the large wind regime where ballistic transport dominates. (In the absence of a good model, the search problem could instead be attacked by model-free reinforcement learning techniques, as in Refs. [23, 24].)

In order to maximize the realism of the model, in this work we study optimal trajectories with respect to likelihoods taken directly from simulation data. In particular,

we examine the trajectories which result from the absence of an encounter; because encounters are rare, in a typical search, most of the search time will be spent in this low-information phase.

The optimal trajectories which we compute are complex and depend strongly on the strength of the mean wind. We focus on the case where the mean wind is strong: in this case the optimal motion is to zigzag up-wind similarly to casting. This motion exhibits characteristic diffusive scaling in both directions. At some critical time, if the searcher has still not found the source, it should return to its starting location. We explain these results using a simple model that assumes encounters are very rare except close to the source. The diffusive scaling is explained by a reduction to the classical linear search problem and is used to predict the arrival time pdf.

METHODS. From the POMDP point of view, the searcher is a Bayesian agent living on a gridworld which maintains a posterior probability density (or “belief”) $b(\mathbf{x})$ over the possible relative positions of the source with respect to the agent; critically, this relative position is unknown. The searcher makes an observation at every timestep, which we define as measuring if the local concentration is above or below some threshold c_{thr} . [In accordance with usual POMDP practice, the observation rate ν_{Ω} is the same as the action rate, i.e. $\nu_{\Omega} = v/\Delta x$, where v is the speed of the searcher and Δx is the grid spacing. In all figures, we will express time in units of ν_{Ω}^{-1} and distance in units of Δx .] The belief is updated in two ways. When the searcher moves (“takes an action” in POMDP jargon), the belief is transported according to $b(\mathbf{x}) \rightarrow b(\mathbf{x} - \delta\mathbf{x})$, where $\delta\mathbf{x}$ is the searcher’s displacement under the action. Secondly, when the searcher makes an observation $\Omega = \theta(c(\mathbf{x}) - c_{\text{thr}})$, it updates its belief according to Bayes’ theorem [25]:

$$b(\mathbf{x}) \rightarrow b(\mathbf{x})p_{\Omega}(\mathbf{x})/Z, \quad (1)$$

where Z is the appropriate normalization constant and we have introduced the notation $p_{\Omega}(\mathbf{x}) \equiv \Pr(\Omega|\mathbf{x})$. The likelihood $p_{\Omega}(\mathbf{x})$ must therefore be assumed to be known to the searcher. In the case where the mean wind $U\hat{x}$ is strong compared to flow velocity fluctuations, it can be modelled as proposed in [15]. The Lagrangian particle motion is predominantly ballistic on the short times relevant to this limit, which facilitates analysis of the tail of the concentration distribution. In particular, the probability that the instantaneous concentration is higher than c_{thr} is

$$p_1(\mathbf{x}) \propto \theta(x)x^{-\alpha} \exp\left[-\left(\frac{Uy}{u_{\text{rms}}x}\right)^2\right] \exp(-x/x_D), \quad (2)$$

where u_{rms} is the typical fluctuation speed of the flow, θ is a Heaviside function, we have supposed the source is in $x = 0$, y is the distance from the plume centerline, $\alpha \geq 0$ is a free parameter that depends on the environment, and x_D is a characteristic decay length which depends on c_{thr} .

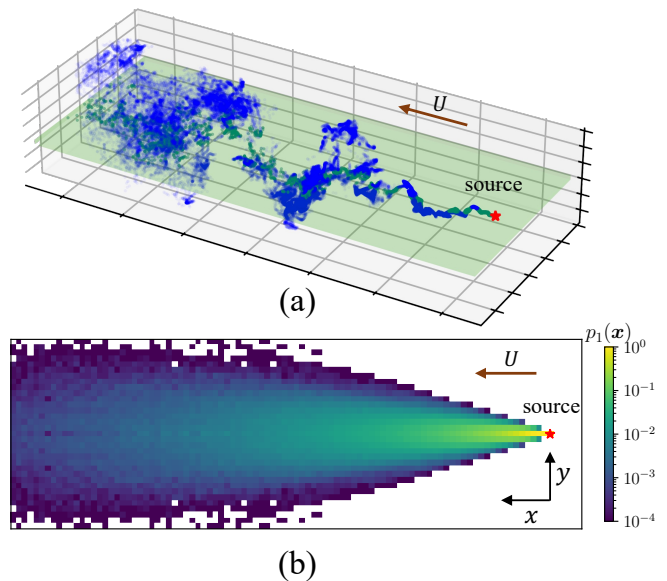


FIG. 1. Upper panel (a): snapshot from the DNS showing particles (blue) and the 2-D slab (green) on which the data are coarse-grained. Lower panel (b): likelihood $p_1(\mathbf{x})$ of an encounter obtained from the DNS for $U/u_{\text{rms}} \simeq 7.4$.

This result is only valid sufficiently far from the source.

On the other hand, when the mean wind is small, long diffusive timescales become relevant to the Lagrangian particle motion and one instead expects

$$p_1(\mathbf{x}) \propto |\mathbf{x}|^{-1} \exp(-|\mathbf{x}|/\lambda) \exp(Ux/2D), \quad (3)$$

with D the effective (Taylor) diffusivity, $\lambda = \sqrt{D\tau/(1 + U^2\tau/4D)}$, and $\tau = \tau(c_{\text{thr}})$ is a typical time for a fluid puff, initially at the source, to grow large enough that the concentration is less than c_{thr} .

Rather than impose one of these models directly, we used empirical models taken from simulations. We performed high-fidelity direct numerical simulations (DNS) of a turbulent flow ($\text{Re}_\lambda \simeq 150$), while tracking the positions of tracer particles which are emitted by a stationary point source. The system is advected by a uniform mean flow $U\hat{x}$; we repeated the simulation for $U/u_{\text{rms}} \in \{0, 1.2, 2.5, 4.9, 7.4\}$. The tracers are taken as proxies for a passive scalar cue; this is a good approximation at high Péclet number. After coarse-graining the particle data onto a 2-D grid of about $\simeq 3250$ cells, we imposed a threshold concentration $c_{\text{thr}} = 200$ particles/cell and computed the likelihood $p_1(\mathbf{x})$ that this threshold is instantaneously exceeded (see Fig. 1). For the largest values of U , the data are a good fit to Eq. 2 with $\alpha = 1$, and for the smallest values of U the data fit Eq. 3 (see Fig. 3 of the Supplemental Material [26]).

For each flow, we then used the SARSOP algorithm [27] to extract a quasi-optimal search policy from the underlying dynamic programming equation [19, 28] (Supplemental Material, Eq. 3 [26]). To study trajectories, we

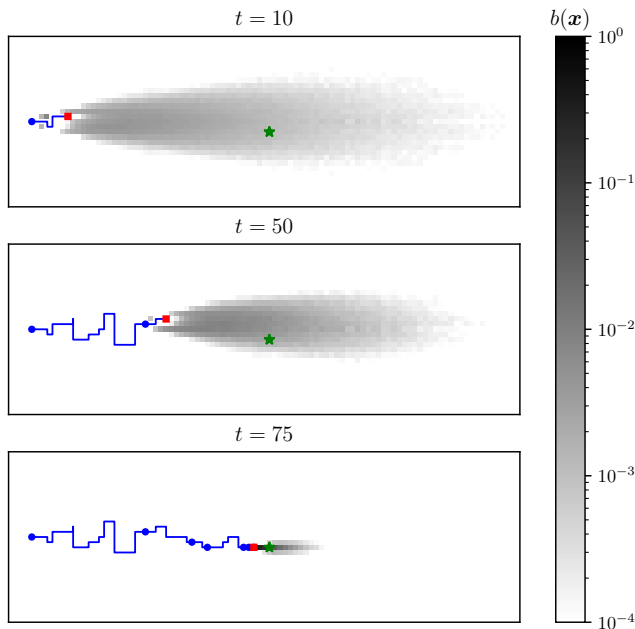


FIG. 2. Snapshots from a trajectory produced from a quasi-optimal policy. The source is shown as a green star and the searcher as a red square. Each encounter is shown as a blue circle. The searcher’s belief $b(\mathbf{x})$ on the position of the source is shown in grayscale. The searcher found the source a couple timesteps after $t = 75$.

generated large ensembles of trajectories via Monte Carlo trials; for comparison, we did the same for the popular heuristic policy “infotaxis” [29], which seeks to minimize the entropy of the posterior.

An important detail is that all trajectories begin with an encounter at time zero, modeling the fact that the searcher has no incentive to search in the absence of an encounter. This induces a prior $b_0(\mathbf{x}) \propto p_1(\mathbf{x})$. To ensure consistency, we begin each trajectory by randomly selecting a source position from the prior. We also constrain the searcher to move in two dimensions, which both eases the computational burden of the POMDP and simplifies the analysis of the results. An example quasi-optimal trajectory is shown in Fig. 2.

RESULTS. Our results can be organized and understood through the following principle: because encounters are rare, the most important optimization the searcher must perform is to decide how it should move when it does not smell anything, and the single most likely trajectory is the one generated in the absence of any encounters after time zero. We will call this deterministic trajectory the “no-hit trajectory.” To support this claim, we evaluated the probability $P_{\text{nh}}(t)$ that, at time t , the searcher has not encountered the cue since time 0, given that it has not yet found the source. This is plotted for the largest wind speed in the upper panel of Fig. 4; the results for other wind speeds are very similar and shown in Figs. 4–5 in the Supplemental Mate-

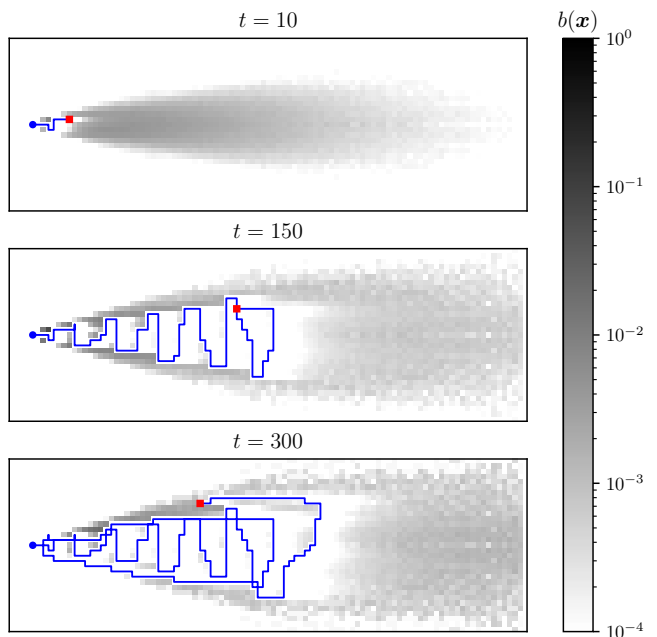


FIG. 3. Quasi-optimal no-hit trajectory, for $U/u_{\text{rms}} \simeq 7.4$. The searcher is shown as a red square, the searcher’s belief is shown in grayscale, and the starting point is a blue circle.

rial [26]. For both quasi-optimal and infotactic motion, $P_{\text{nh}}(t) \gtrsim 0.5$ for all times t , so the no-hit trajectory plays an outside role.

We find that when the mean wind is strong, the quasi-optimal no-hit trajectory begins by moving slowly upwind while zigzagging in the crosswind direction (Fig. 3). This motion strongly resembles casting. However, at some critical time, the searcher ceases this behavior and returns downwind to the vicinity of its starting position. From then on, the motion is dominated by upwind and downwind motion. Downwind returns have also been occasionally observed in wind-tunnel experiments after a long time without an encounter [30, 31], but this behavior is far less well-known. In contrast, infotaxis produces almost pure zigzagging motion in the absence of an encounter, and essentially never executes a downwind return.

Other examples of no-hit trajectories are supplied in Secs. VI C–D of the Supplemental Material [26]. As the wind speed decreases, the downwind return occurs earlier and earlier, and zigzagging quickly becomes irrelevant to the optimal motion. Instead, at moderate wind speed, a quasi-optimal searcher exhibits repeated up- and downwind motion that begins to resemble a complex, asymmetric spiral. We suggest that the curves tend to approximately lie on isolines of the prior, which would imply the trajectories are essentially performing gradient ascent of the likelihood profile. When U and u_{rms} are comparable, the problem has very little symmetry and, accordingly, the trajectories are especially complex. At $U = 0$, both the quasi-optimal and infotaxis trajectories

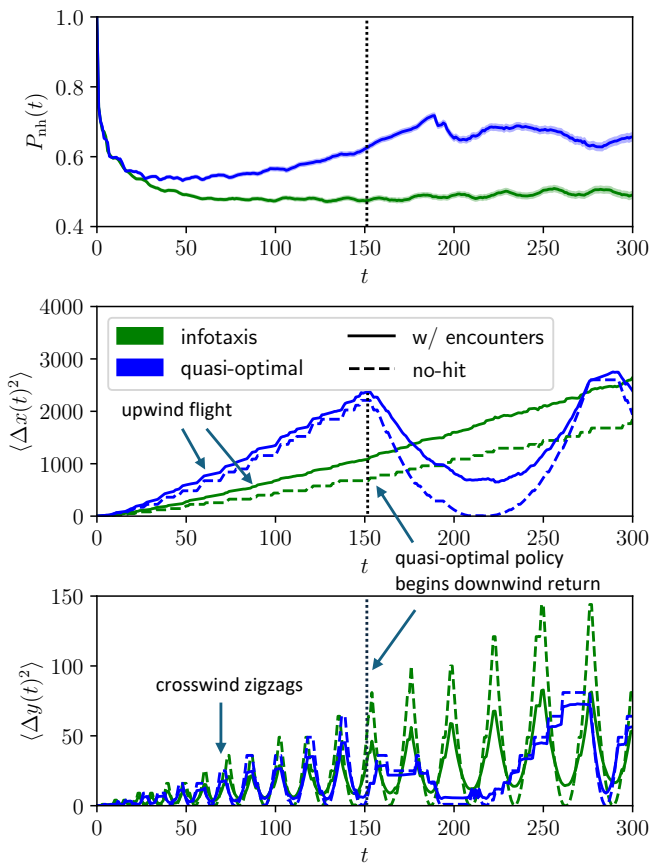


FIG. 4.

resemble Archimedean spirals, consistent with previous studies [20, 29, 32].

These behaviors generate clear signatures in the mean squared displacement (MSD) of the searcher, $\langle \Delta x(t)^2 \rangle \equiv \langle (x(t) - x(0))^2 \rangle$ and $\langle \Delta y(t)^2 \rangle \equiv \langle (y(t) - y(0))^2 \rangle$, of the searcher, which we plot in Fig. 4 (lower panels). These are averaged over an ensemble of 10^4 trajectories, and compared with the squared displacements resulting from a no-hit trajectory. The results are very similar, suggesting that motion in absence of an encounter is dominating the MSD signal. For the larger values of U , the MSD in y exhibits fast oscillations, the amplitude of which grows like t . The MSD in x also grows approximately linearly. These results imply that the rms displacement envelopes in both x and y exhibit diffusive scaling: $x, y \sim t^{1/2}$.

In the same figure, we also show the MSD resulting from an infotactic trajectory. While both infotaxis and quasi-optimal policy show the same behavior at small times, there is a clear qualitative difference at larger times: for the quasi-optimal policy, at some critical time, the oscillations and linear scaling cease, and from $t \simeq 150$ – 200 the MSD in x decays rapidly like t^2 , consistent with a ballistic downwind return. The time elapsed before returning becomes smaller as U decreases (see Supplemental Material, Secs. VI A, C, D [26]), and eventually the zigzag oscil-

lations disappear completely. The infotactic policy, on the other hand, always produces an almost pure zigzag motion, except at the smallest nonzero value of U .

LOW-INFORMATION LIMIT. The results at large wind speed can be understood by means of a simplified model. In particular, we again assume the searcher initializes its belief as the prior $b_0(\mathbf{x})$ induced by the encounter at time zero, i.e., proportional to Eq. 2 for large enough x . However, consistent with the dominance of the no-hit trajectory, we assume successive encounters only occur when the searcher is close to the source—the likelihood is very close to unity in a strip directly downwind of the source (see yellow region in Fig. 1, lower panel), which is where $\langle c \rangle > c_{\text{thr}}$. Empirically, this strip has negligible length except when U is large;

Explicitly, we model the likelihood of an encounter after time $t = 0$ as

$$p_1(\mathbf{x}) = \begin{cases} 1, & 0 < x < \ell^*, y = 0 \\ 0, & \text{otherwise,} \end{cases} \quad (4)$$

where x and y are, respectively the upwind and crosswind position of the source with respect to the searcher, and ℓ^* is the characteristic length of the strip. The searcher uses this likelihood to update its belief. We will call this simplified model the *low-information limit*. A similar model was used to describe sector search in Ref. [33].

In this limit, the result of the Bayesian update (Eq. 1) is that the searcher will simply zero out its prior in a ℓ^* -neighborhood (and renormalize) as it moves (see Fig. 5, panel (a)). The optimal trajectory will then be the one that most efficiently explores the prior’s support, so the geometry of the prior plays an essential role.

We now determine the optimal trajectories in the low-information limit. Due to the Gaussian factor in Eq. 2, the prior will be strongly confined to a cone C given by $|y| < ax$ with $a \sim u_{\text{rms}}/U$, so it is useful to approximate the confinement as exact: suppose the prior depends only on x inside the cone, and it is zero outside (see Fig. 5, panel (a)). We seek to minimize the expected time of arrival

$$J = \frac{1}{2a} \int_{-a}^a du \int_0^\infty dx p(x) T(x, u),$$

where $u \equiv y/x$, $T(\cdot)$ is the time that the searcher first sweeps out a given point in space, and $p(x) \equiv x b_0(x)$.

As a first observation, if $p(x)$ decays monotonically, then the optimal trajectory should (on average) visit states in order of increasing x [34]. Second, the searcher should make as few turning points in y as possible, since no probability mass is swept out if $dy/dt = 0$. Therefore it is reasonable to assume the only turning points occur at the edges of the cone. Such a trajectory will necessarily look like an upwind zigzag, but we have not yet determined the scalings of x and y with time.

A zigzag trajectory can be (for large enough x) mod-

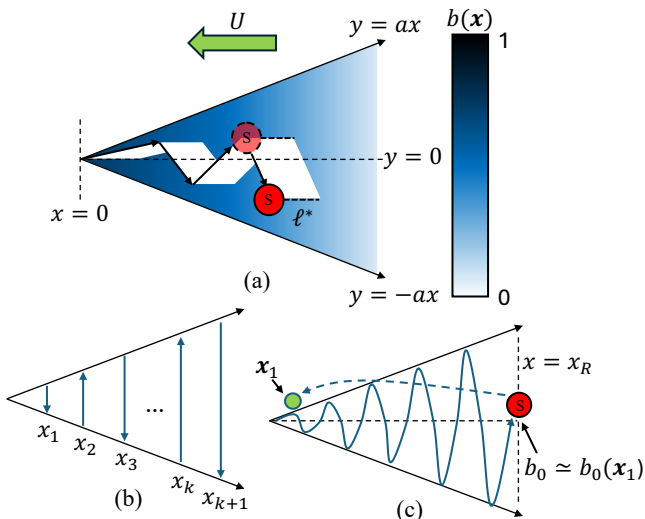


FIG. 5. Upper panel (a): in the simplified model, the prior decays as a function of x and is only supported on a cone symmetric about the x -axis. The searcher (red circle, labeled “S”) sweeps out probability mass in the upwind direction as it moves, over a characteristic length ℓ^* . Lower left panel (b): a zigzag trajectory may be approximated by a sequence of crosswind motions at upwind distances x_k , and the decision problem reduces to selecting the x_k . Lower right panel (c): when the searcher has swept out the cone up to an upwind distance $x_R \sim x_D$, the local value of the prior b_0 is comparable to that near the starting point and just outside the cone, \mathbf{x}_1 . The searcher should return to \mathbf{x}_1 .

eled by a sequence of purely crosswind moves at positions x_1, x_2, \dots (see Fig. 5, panel (b)). A key observation is that the searcher should not move further upwind than ℓ^* during any crosswind traversal, i.e., we have the constraint $x_{k+1} - x_k \leq \ell^*$ for each k . Otherwise, there will be points not swept out by the trajectory, and because the trajectory is monotonic in x , J will be infinite.

In the absence of the inequality constraint, the decision problem of choosing the optimal sequence $\{x_k\}$ is exactly equivalent to the linear search problem (LSP), a well-studied decision problem which asks for the turning points of a trajectory on a line which minimizes the expected arrival time to a target drawn from some known probability density [35–38]. This is shown in the Supplemental Material (Sec. V), after which we prove that if $p(x)$ decays exponentially or slower—as it does in our case—then $x_{k+1} - x_k$ asymptotically diverges for large k [26]. Thus the inequality constraint must saturate far enough upwind, i.e., $x_{k+1} - x_k = \ell^*$, and one can show this gives rise to diffusive scaling as observed in the MSD data.

(ignoring numerical factors)

$$x(t) \sim \sqrt{\frac{\ell^* v U t}{u_{\text{rms}}}}; \quad y(t) \sim \sqrt{\frac{\ell^* v u_{\text{rms}} t}{U}} \cos \sqrt{\frac{v U t}{\ell^* u_{\text{rms}}}}, \quad (5)$$

with asymptotically constant speed $\sim v$ in an rms sense.

We therefore conclude that the zigzag motion with $t^{1/2}$ scaling is a consequence of the fact that (a) the likelihood decays exponentially with x (and not faster), (b) the likelihood decays faster than exponential outside the cone, and (c) the likelihood is small outside of a strip in front of the source. However, the argument (in particular, point (b)) rests on the approximation $\exp[-(u_{\text{rms}} y / U x)^2] \ll \exp(-x/x_D)$. When the searcher reaches an upwind distance $x_R \sim x_D$, this approximation breaks down, and the local prior probability will be comparable to that just outside the cone, near the starting point (see Fig. 5, panel (c)). This means that there is no continued benefit to search upwind, and the searcher should instead return downwind—as we indeed observe in the quasi-optimal policy.

We cannot analytically predict the optimal trajectories at finite U (and moreover the approximation Eq. 4 becomes untenable), but the low-information limit still grants some insights. Using the analysis of Ref. [15], one expects $x_D \sim u_{\text{rms}}^{-1} (S U / c_{\text{thr}})^{1/2}$ (where S is the emission rate) when U is large enough that ballistic single- and two-particle dispersion scaling still holds on relevant timescales. This is in basic agreement with our observation that downwind returns occur earlier as U decreases. Eventually, as U becomes comparable to u_{rms} , diffusive motion begins to dominate trajectories of Lagrangian particles on timescales of interest. In this regime, the likelihood is no longer well-confined to a cone and gains some support even upwind of the source (this is visible in our simulations at $U/u_{\text{rms}} \simeq 1.2$). This complexification of the prior geometry leads to concomitantly complex optimal trajectories (see Supplemental Material, Sec. VI A, C, D [26]).

Finally, a useful consequence of the $t^{1/2}$ scaling at large U is that it allows us to predict the tail of the arrival time pdf analytically. In the low-information limit, the arrival time is dominated by the time of the first encounter after $t = 0$, which is the time it takes to reach a ℓ^* -neighborhood of the source. Therefore, we can estimate the arrival time pdf $p(T)$ as

$$p(T) = \int d^2 \mathbf{x} b_0(\mathbf{x}) \delta(T - T^*(\mathbf{x})), \quad (6)$$

where $T^*(\mathbf{x})$ is the time that the optimal trajectory first reaches \mathbf{x} . $b_0(\mathbf{x})$ is proportional to the likelihood, which is given by Eq. 2 for large U , and we have from Eq. 5 that $T^*(x, y) \sim (u_{\text{rms}}/U)(x^2/v\ell^*)$. This gives

$$p(T) \propto T^{-\alpha/2} \exp(-k\sqrt{T}), \quad (7)$$

with $k \sim x_D^{-1} \sqrt{U v \ell^* / u_{\text{rms}}}$, a new prediction.

In Fig. 6 we plot the pdf of \sqrt{T} for $U/u_{\text{rms}} \simeq 7.4$, where T is the time of arrival. There is a broad range $0 \leq T \lesssim 500$ where the pdf appears to decay exponentially, implying $p(T) \sim \exp(-k\sqrt{T})$ as predicted. The agreement with exponential decay is more precise for infotaxis; we could have anticipated this since infotaxis was

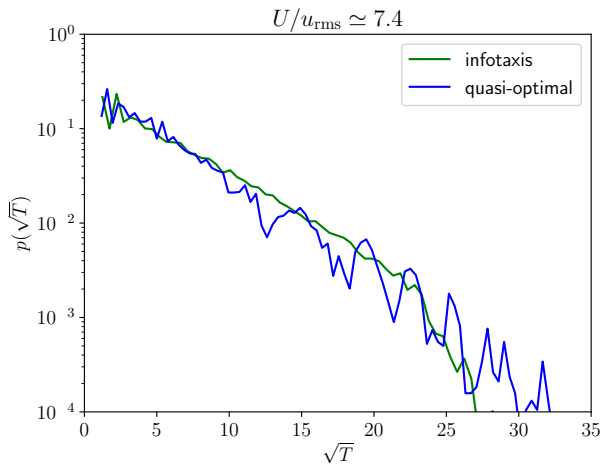


FIG. 6. Pdf of the square root of the arrival time \sqrt{T} , for $U/u_{\text{rms}} \simeq 7.4$, obtained using 10^5 Monte Carlo trials.

observed to obey $t^{1/2}$ scaling for the entire trajectory, whereas this scaling breaks down for the quasi-optimal policy once it begins its downwind return.

In summary, our results suggest that the ubiquity of casting as a response to loss of plume contact may be due to its being the optimal no-hit trajectory in the limit

of low information, in the presence of strong mean wind. The same limit makes nontrivial quantitative predictions about the temporal scaling of the trajectories and the arrival time pdfs, which agree with results obtained using quasi-optimal policies extracted from the dynamic programming equation.

ACKNOWLEDGMENTS

We thank Aurore Loisy, Massimo Cencini, Lorenzo Piro, and Fabio Bonaccorso for fruitful discussions and acknowledge useful interactions at the 2023 Les Houches summer school on turbulence. This work received funding from the European Union’s Horizon 2020 Program under grant agreement No. 882340. We also acknowledge financial support under the National Recovery and Resilience Plan (NRRP), Mission 4, Component 2, Investment 1.1, Call for tender No. 104 published on 2.2.2022 by the Italian Ministry of University and Research (MUR), funded by the European Union – NextGenerationEU – Project Title Equations informed and data-driven approaches for collective optimal search in complex flows (CO-SEARCH), Contract 202249Z89M. – CUP B53D23003920006 and E53D23001610006.

-
- [1] F. Roozen and M. Lüring, Behavioural response of daphnia to olfactory cues from food, competitors and predators, *Journal of Plankton Research* **23**, 797 (2001).
 - [2] E. Álvarez-Salvado, A. M. Licata, E. G. Connor, M. K. McHugh, B. M. King, N. Stavropoulos, J. D. Victor, J. P. Crimaldi, and K. I. Nagel, Elementary sensory-motor transformations underlying olfactory navigation in walking fruit-flies, *Elife* **7**, e37815 (2018).
 - [3] A. Thesen, J. B. Steen, and K. Doving, Behaviour of dogs during olfactory tracking, *Journal of Experimental Biology* **180**, 247 (1993).
 - [4] G. Reddy, V. N. Murthy, and M. Vergassola, Olfactory sensing and navigation in turbulent environments, *Annual Review of Condensed Matter Physics* **13** (2022).
 - [5] R. Cardé and T. Hagaman, Behavioral responses of the gypsy moth in a wind tunnel to air-borne enantiomers of disparlure, *Environmental Entomology* **8**, 475 (1979).
 - [6] J. Kennedy, A. Ludlow, and C. Sanders, Guidance of flying male moths by wind-borne sex pheromone, *Physiological Entomology* **6**, 395 (1981).
 - [7] J. Elkinton, C. Schal, T. Onot, and R. Cardé, Pheromone puff trajectory and upwind flight of male gypsy moths in a forest, *Physiological Entomology* **12**, 399 (1987).
 - [8] J. Murlis, J. S. Elkinton, and R. T. Carde, Odor plumes and how insects use them, *Annual review of entomology* **37**, 505 (1992).
 - [9] D. Martinez, O. Rochel, and E. Hugues, A biomimetic robot for tracking specific odors in turbulent plumes, *Autonomous Robots* **20**, 185 (2006).
 - [10] D. Martinez and E. M. Moraud, Reactive and cognitive search strategies for olfactory robots, *Neuromorphic Olfaction* **5**, 153 (2013).
 - [11] H. G. Nguyen, A. Nans, K. Talke, P. Candela, and H. Everett, Automatic behavior sensing for a bomb-detecting dog, in *Unmanned Systems Technology XVII*, Vol. 9468 (SPIE, 2015) pp. 138–146.
 - [12] T. Wiedemann, A. J. Lilienthal, and D. Shutin, Analysis of model mismatch effects for a model-based gas source localization strategy incorporating advection knowledge, *Sensors* **19**, 520 (2019).
 - [13] E. Yee, P. Kosteniuk, G. Chandler, C. Bilotto, and J. Bowers, Statistical characteristics of concentration fluctuations in dispersing plumes in the atmospheric surface layer, *Boundary-Layer Meteorology* **65**, 69 (1993).
 - [14] E. Balkovsky and B. I. Shraiman, Olfactory search at high Reynolds number, *Proceedings of the National Academy of Sciences* **99**, 12589 (2002).
 - [15] A. Celani, E. Villermaux, and M. Vergassola, Odor landscapes in turbulent environments, *Physical Review X* **4**, 041015 (2014).
 - [16] B. I. Shraiman and E. D. Siggia, Scalar turbulence, *Nature* **405**, 639 (2000).
 - [17] J. Kennedy, Zigzagging and casting as a programmed response to wind-borne odour: a review, *Physiological Entomology* **8**, 109 (1983).
 - [18] S. A. Budick and M. H. Dickinson, Free-flight responses of *Drosophila melanogaster* to attractive odors, *Journal of experimental biology* **209**, 3001 (2006).
 - [19] L. P. Kaelbling, M. L. Littman, and A. R. Cassandra, Planning and acting in partially observable stochastic do-

- mains, *Artificial intelligence* **101**, 99 (1998).
- [20] A. Loisy and C. Eloy, Searching for a source without gradients: how good is infotaxis and how to beat it, *Proceedings of the Royal Society A* **478**, 20220118 (2022).
- [21] R. A. Heinonen, L. Biferale, A. Celani, and M. Vergassola, Optimal policies for Bayesian olfactory search in turbulent flows, *Physical Review E* **107**, 055105 (2023).
- [22] A. Loisy and R. A. Heinonen, Deep reinforcement learning for the olfactory search POMDP: a quantitative benchmark, *The European Physical Journal E* **46**, 17 (2023).
- [23] S. H. Singh, F. van Breugel, R. P. Rao, and B. W. Brunton, Emergent behaviour and neural dynamics in artificial agents tracking odour plumes, *Nature Machine Intelligence* **5**, 58 (2023).
- [24] M. Rando, M. James, A. Verri, L. Rosasco, and A. Seminara, Q-learning to navigate turbulence without a map (2024), arXiv:2404.17495.
- [25] G. E. Box and G. C. Tiao, *Bayesian inference in statistical analysis* (John Wiley & Sons, 2011).
- [26] See Supplemental Material at [hyperlink], which includes Refs. [43, 44] for detailed information about methods for the DNS and POMDP solution, as well as additional calculations, plots, and movies.
- [27] H. Kurniawati, D. Hsu, and W. S. Lee, Sarsop: Efficient point-based POMDP planning by approximating optimally reachable belief spaces., in *Robotics: Science and systems*, Vol. 2008 (Citeseer, 2008).
- [28] E. J. Sondik, The optimal control of partially observable markov processes over the infinite horizon: Discounted costs, *Operations research* **26**, 282 (1978).
- [29] M. Vergassola, E. Villermanx, and B. I. Shraiman, ‘Infotaxis’ as a strategy for searching without gradients, *Nature* **445**, 406 (2007).
- [30] M. A. Willis and E. A. Arbas, Odor-modulated upwind flight of the sphinx moth, *manduca sexta* l., *Journal of Comparative Physiology A* **169**, 427 (1991).
- [31] L. Kuenen and R. T. Carde, Strategies for recontacting a lost pheromone plume: casting and upwind flight in the male gypsy moth, *Physiological Entomology* **19**, 15 (1994).
- [32] C. Barbieri, S. Cocco, and R. Monasson, On the trajectories and performance of infotaxis, an information-based greedy search algorithm, *EuroPhysics letters* **94**, 20005 (2011).
- [33] G. Reddy, B. I. Shraiman, and M. Vergassola, Sector search strategies for odor trail tracking, *Proceedings of the National Academy of Sciences* **119**, e2107431118 (2022).
- [34] To see this, note that if $x_2 > x_1$ but $\int_{-a}^a du T(x_1, u) > \int_{-a}^a du T(x_2, u)$, a new assignment of arrival times \tilde{T} with $\tilde{T}(x_1) = T(x_2)$, $\tilde{T}(x_2) = T(x_1)$, and $\tilde{T}(x) = T(x)$ otherwise will result in a smaller value of J .
- [35] A. Beck, On the linear search problem, *Israel Journal of Mathematics* **2**, 221 (1964).
- [36] A. Beck and M. Beck, Son of the linear search problem, *Israel Journal of Mathematics* **48**, 109 (1984).
- [37] A. Beck and M. Beck, The linear search problem rides again, *Israel Journal of Mathematics* **53**, 365 (1986).
- [38] S. Alpern and S. Gal, *The theory of search games and rendezvous*, International Series in Operations Research & Management Science, Vol. 55 (Springer Science & Business Media, 2003).
- [39] S. Guichard, D. Kriticos, A. Leriche, S. Worner, J. Kean, and D. M. Suckling, Evidence of active or passive downwind dispersal in mark–release–recapture of moths, *Entomologia Experimentalis et Applicata* **134**, 160 (2010).
- [40] S. D. Stupski and F. van Breugel, Wind gates olfaction-driven search states in free flight, *Current Biology* **34**, 4397 (2024).
- [41] F. Bonaccorso, R. A. Heinonen, N. Cocciaglia, and L. Biferale, Turb-Odor dataset, Smart-Turb database (2025).
- [42] R. A. Heinonen, OlfactorySearch software, GitHub (2025).
- [43] G. Shani, J. Pineau, and R. Kaplow, A survey of point-based POMDP solvers, *Autonomous Agents and Multi-Agent Systems* **27**, 1 (2013).
- [44] M. T. Spaan and N. Vlassis, Perseus: Randomized point-based value iteration for POMDPs, *Journal of artificial intelligence research* **24**, 195 (2005).

Supplemental Material: Optimal trajectories for Bayesian olfactory search in turbulent flows: the low information limit and beyond

R. A. Heinonen,¹ L. Biferale,¹ A. Celani,² and M. Vergassola³

¹*Dept. Physics and INFN, University of Rome “Tor Vergata”,
Via della Ricerca Scientifica 1, 00133 Rome, Italy*

²*Quantitative Life Sciences, The Abdus Salam International Centre for Theoretical Physics, 34151 Trieste, Italy*

³*Laboratoire de physique, École Normale Supérieure, CNRS,
PSL Research University, Sorbonne University, Paris 75005, France*

I. METHODS

A. DNS

In order to obtain realistic encounter likelihoods, we solved the incompressible, 3-D Navier-Stokes equations

$$\partial_t \mathbf{u} + (\mathbf{u} \cdot \nabla) \mathbf{u} = -\nabla p + \nu \nabla^2 \mathbf{u} + f, \quad (1)$$

$$\nabla \cdot \mathbf{u} = 0, \quad (2)$$

under turbulent conditions with $\text{Re}_\lambda \simeq 150$. Here, f is a random isotropic forcing at the smallest nonzero wavenumbers of the system, with a correlation time of 160 simulation timesteps, or approximately one Kolmogorov time τ_η . Using a pseudospectral code dealiased according to the two-thirds rule, the system was solved on a $1024 \times 512 \times 512$ grid, with a uniform spacing $\delta x = \delta y = \delta z \simeq \eta$ (with η the Kolmogorov scale), and periodic boundary conditions in all three directions. The timestepping was performed using the second-order explicit Adams-Bashforth method. The system was advected by a uniform mean wind $\mathbf{U} \approx -2.5u_{\text{rms}}\hat{x}$, where u_{rms} is the rms speed of the flow in the comoving frame of the wind, and \hat{x} is the elongated axis of the grid. We produced the mean wind by means of a Galilean transformation.

Five stationary point sources each emitted 1000 Lagrangian tracer particles every 10 simulation timesteps, which corresponds to every $\approx 1/15\tau_\eta$. The fluid velocities \mathbf{u} at the particle positions were obtained using a sixth-order B-spline interpolation scheme and then used to evolve the particle positions \mathbf{X} in time according to $\dot{\mathbf{X}} = \mathbf{u}(\mathbf{X}, t)$ over an infinite lattice of copies of the periodic flow. Their positions, velocities, and accelerations were tracked and dumped every τ_η , for a total of about 3000 timesteps. Each source of particles was treated as independent, and we averaged our results over them for the purpose of achieving better statistics.

The particle data were then coarse-grained onto a quasi-two-dimensional slab which contained the source and was parallel to the wind. The slab comprised $\simeq 3250$ cubic cells with side length $\simeq 15\eta$ (here, η is the Kolmogorov length); the aspect ratio of the grid depended on the wind speed and was chosen to ensure the likelihood was $< 10^{-4}$ at the boundary. The likelihoods were computed as the time averaged probability that the number of particles in a given cell exceeded threshold. In the presence of wind, these were symmetrized along the wind axis; in the isotropic case, they were symmetrized to be a function of r only. We show likelihoods for all windspeeds in Figs. 1–2.

B. POMDP details

The POMDP was setup similarly to Refs. [1–3], to which we refer the interested reader for details. The agent lived on the gridworld defined in the previous subsection, and the source was fixed at an unknown location. Its belief b

states	agent position \mathbf{x} w.r.t. source in gridworld
actions	move to an adjacent gridpoint
state transitions	deterministic, determined by actions
observations	binary (above/below threshold) concentration measurements
reward	unit penalty per timestep until source reached
prior (initial belief)	induced by encounter at time zero

TABLE I: Summary of olfactory search POMDP.

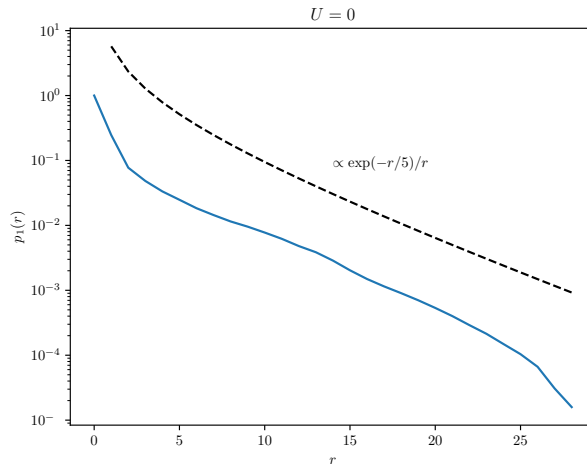


FIG. 1: Symmetrized empirical likelihood $p_1(r)$ of encounter in isotropic setting. For comparison, we also show a diffusive model, which fits reasonably well.

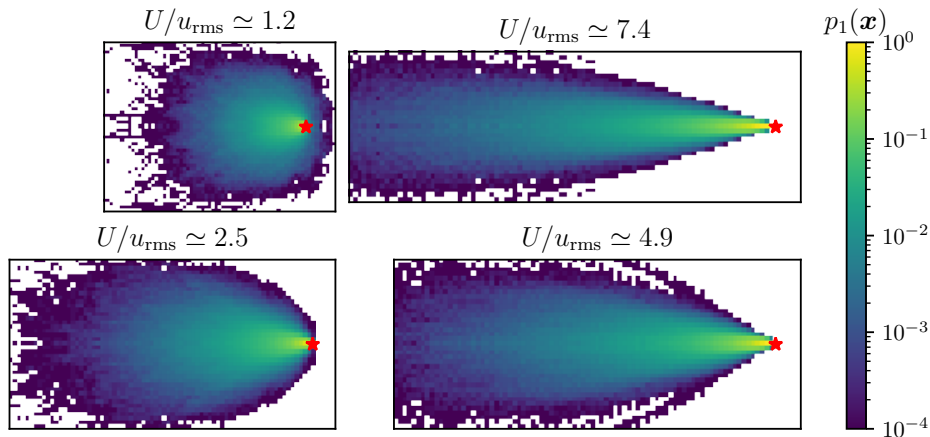


FIG. 2: Empirical likelihoods $p_1(\mathbf{x})$ of encounter in the presence of a mean wind U .

was a probability distribution over all possible relative positions between the source and agent; these positions are the states of the POMDP. At each timestep the agent drew a binary observation from the likelihood, which was used to update its belief via Bayes’ theorem. The agent then took an action, defined as moving to one of the four adjacent grid cells (at the boundary, actions which would take the agent out of the gridworld were excluded). The motion of the agent was treated as deterministic (i.e. the agent successfully moved to the intended grid point with probability one).

Monte Carlo trials were initialized by placing the agent at a chosen starting location, setting the prior by triggering an encounter at time zero, and drawing the relative position of the source from the prior for self-consistency. The trials terminated when the agent arrived at the source, or if the agent had still not arrived after 2500 timesteps.

The reward function was modeled as a unit penalty per timestep until the source was reached. The state transitions, observation likelihood, reward function, and choice of prior (see Table I for a summary) were then used as inputs into the SARSOP algorithm [4], which approximately solves the dynamic programming equation, also called the Bellman equation [5, 6]. This equation expresses the recursive structure of the “value function” $V(b)$, which returns the total expected reward conditioned on the current belief being b . For our problem it reads

$$V(b) = -1 + \gamma \max_{\mathbf{a} \in A} \sum_{\Omega \in \{0,1\}} \Pr(\Omega|b, \mathbf{a}) V(b'(\cdot|\Omega, \mathbf{a})), \quad (3)$$

walltime (s)	$\langle T \rangle$	$\langle R \rangle$
30	49.31 \pm 0.86	19.67 \pm 0.16
100	46.83 \pm 0.85	19.32 \pm 0.16
300	47.34 \pm 0.85	19.58 \pm 0.16
1000	46.64 \pm 0.83	19.28 \pm 0.16
2000	45.47 \pm 0.81	19.34 \pm 0.16
4000	44.58 \pm 0.76	19.29 \pm 0.15
6000	44.86 \pm 0.79	19.08 \pm 0.16
8000	44.61 \pm 0.79	19.15 \pm 0.15
10000	45.67 \pm 0.83	19.23 \pm 0.15

TABLE II:

where $\gamma \in (0, 1]$ is the discount factor, which geometrically suppresses future rewards in favor of immediate ones, Ω is an observation, A is the set of four possible actions, $b'(\cdot|\Omega, \mathbf{a})$ refers to the belief obtained after taking action \mathbf{a} , observing Ω , and then applying a Bayesian update to b , and

$$\Pr(\Omega|b, \mathbf{a}) = \sum_{\mathbf{x}} p_{\Omega}(\mathbf{x} + \mathbf{a})b(\mathbf{x}), \quad (4)$$

with p_{Ω} the likelihood as defined in the main text. Knowledge of $V(b)$ immediately yields the optimal policy $\pi^*(b)$, which is just the maximizing action on the RHS of Eq. 3.

SARSOP obtains an approximation for the value function

$$V(b) \simeq \max_k b \cdot \boldsymbol{\alpha}_k, \quad (5)$$

where the dot product indicates a product and sum over state indices, and $\{\boldsymbol{\alpha}_k\}$ is a collection of matrices with the same dimension as the state space. Each $\boldsymbol{\alpha}_k$ comes equipped with an associated action a_k , and the (quasi-)optimal policy selects the action associated with the maximizing $\boldsymbol{\alpha}_k$.

The SARSOP algorithm requires $\gamma < 1$; we took $\gamma = 0.98$, as close to unity as possible without compromising the successful convergence of the algorithm.

II. ESTIMATE OF LIKELIHOOD FOR SMALL MEAN WIND

In the Lagrangian picture, the concentration due to a continuously-emitting point source at the origin with emission rate S is [9]

$$c(\mathbf{x}) = S \int_0^{\infty} dt \Pr(\mathbf{X}(t) = \mathbf{x} | \mathbf{X}(0) = 0). \quad (6)$$

$\Pr(\mathbf{X}(t) = \mathbf{x} | \mathbf{X}(0) = 0)$ is the probability that a Lagrangian particle starting at the origin arrives at the test point \mathbf{x} at time t and is generally represented by a path integral. The integration variable t then represents how long in the past the particle was released. In the large mean wind limit, one may exploit the ballistic scaling of the particles to only consider the contribution from times $t = x/U$, which greatly simplifies the analysis and leads to the results of Ref. [10].

However, if the mean wind is small, all past times contribute to the concentration and the calculation is in principle quite involved. In particular, we are interested in the tail of the distribution of $c(\mathbf{x})$.

To estimate $p_1(\mathbf{x}) = \Pr(c > c_{\text{thr}} | \mathbf{x})$ for large c_{thr} , we assume large fluctuations in the concentration are due to a puff released from the source remaining small for a much longer time than usual. Fluid velocity fluctuations on the scale of the puff size will tend to disperse the puff, increasing its radius and thereby decreasing the local concentration. The probability that the puff remains small some time $t^* \gg \tau$, where $\tau = \tau(c_{\text{thr}})$ is the typical time for the concentration of the puff to be reduced below c_{thr} , will be the product of many largely independent factors, leading to Poisson

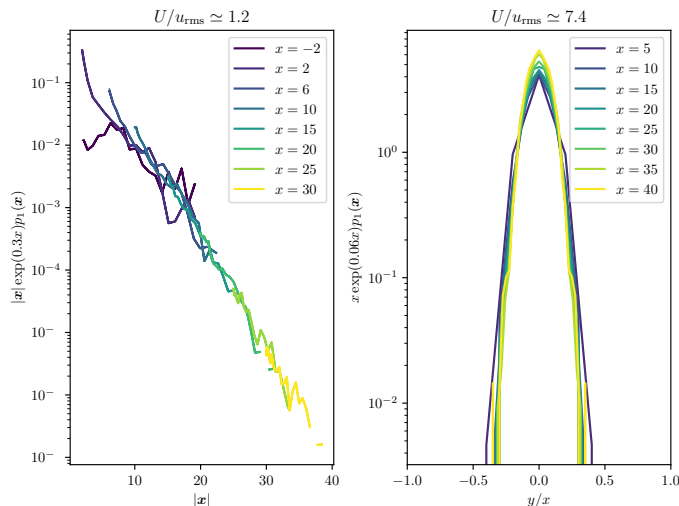


FIG. 3: Left panel: collapse of likelihood to a model of the form Eq. 8, for the smallest wind speed $U/u_{\text{rms}} \simeq 1.2$. Right panel: collapse of likelihood to a model of the form Eq. 9 with $\alpha = 1$ for the largest wind speed $U/u_{\text{rms}} \simeq 7.4$.

statistics and a tail of the form $p(t^*) \sim \exp(-t^*/\tau)$. This gives

$$\Pr(c > c_{\text{thr}}|\mathbf{x}) \simeq S \int_0^\infty dt \int_t^\infty dt^* p(t^*) \Pr(\mathbf{X}(t) = \mathbf{x} | \mathbf{X}(0) = 0). \quad (7)$$

At sufficiently large t , the particle motion decorrelates and passes from ballistic to diffusive, leading to

$$\Pr(\mathbf{X}(t) = \mathbf{x} | \mathbf{X}(0) = 0) = (4\pi Dt)^{-3/2} \exp(-|\mathbf{x} - \mathbf{U}t|^2/4Dt)$$

for a characteristic diffusivity D . This leads to

$$p_1(\mathbf{x}) \propto |\mathbf{x}|^{-1} \exp(-|\mathbf{x}|/\lambda) \exp(Ux/2D), \quad (8)$$

with $\lambda = \sqrt{D\tau/(1 + U^2\tau/4D)}$. This is proportional to the solution of the advection diffusion equation

$$\partial_t p_1 + U \partial_x p_1 = D \nabla^2 p_1 + S \delta(\mathbf{x}).$$

III. COLLAPSE OF EMPIRICAL LIKELIHOODS TO MODELS

In the left panel of Fig. 3, we show that the likelihood at the smallest wind speed $U/u_{\text{rms}} \simeq 1.2$ is a good fit to a model of the form Eq. 8, indicating that diffusive effects are dominant. On the other hand, the right panel shows the collapse of the likelihood for the largest wind speed $U/u_{\text{rms}} \simeq 7.4$ onto a model of the form

$$p_1(\mathbf{x}) = x^{-\alpha} \exp(-x/x_0) \exp\left[-c \left(\frac{y}{x}\right)^2\right], \quad (9)$$

for $x > 0$ (downwind), as predicted in Ref. [10] and discussed in the main text. In particular, the data are a good fit to $\alpha = 1$.

IV. ANALYSIS OF LINEAR SEARCH PROBLEM

A. Reduction to linear search

We first note that the conical search problem, treated in the main text as a model for the $U/u_{\text{rms}} \rightarrow \infty$ limit, is topologically the same as the search problem on the isotropic (i.e., $U = 0$) plane, with a cut along a semiaxis, under

the identification $x \leftrightarrow r, u \leftrightarrow \theta, a \leftrightarrow \pi$ (where r and θ are the polar coordinates in the plane). Zigzag trajectories with $t^{1/2}$ scaling in the former correspond to Archimedean spirals in the latter. We find the isotropic problem is a bit more convenient to study; our goal is to show that the trajectory is an Archimedean spiral.

Let the (isotropic) prior be $b_0(r)$. Put $p(r) = 2\pi r b_0(r)$ so that $\int dr p(r) = 1$. Assume $p(r)$ decreases monotonically, has finite mean, and is nonzero everywhere. The polar coordinates of the source are (r^*, θ^*) drawn respectively from $b_0(r)$ and a uniform distribution on $[0, 2\pi)$. The agent finds the source when its coordinates (r, θ) satisfy $\theta = \theta^*$ and $|r - r^*| < \ell^*/2$, where ℓ^* is the characteristic length swept out by the agent (see Fig. 6 in the main text).

Analogizing the arguments of the main text, the agent should follow a trajectory monotonic in r and with no turning points in θ . This means the trajectory is a spiral and can be parametrized as $r = r(\theta)$. We also have the constraint

$$r(\theta + 2\pi) \leq r(\theta) + \ell^* \quad (10)$$

or $\langle r'(\theta) \rangle \leq \ell^*$.

When $r \gg \ell^*$ we have

$$v^2 = \dot{r}^2 + r^2 \dot{\theta}^2 = \dot{\theta}^2 (r'(\theta)^2 + r^2) \simeq r^2 \dot{\theta}^2,$$

so the motion is in the $\hat{\theta}$ direction, and the trajectory may be approximated by a sequence of concentric circles.

Asymptotically, the decision problem may then be approximately reduced to choosing a discrete sequence of radii r_k and sweeping out each circle $r = r_k$. The objective function for the r_k is then

$$\begin{aligned} J &= \sum_{k=1}^{\infty} \int_{r_{k-1} + \ell^*/2}^{r_k + \ell^*/2} dr p(r) \left[\pi r_k + 2\pi \sum_{j=1}^{k-1} r_j \right] \\ &= \sum_{k=1}^{\infty} \int_{\tilde{r}_{k-1}}^{\tilde{r}_k} dr p(r) \left[\pi \tilde{r}_k + 2\pi \sum_{j=1}^{k-1} \tilde{r}_j \right] + \text{const.} \\ &= \pi \sum_{k=1}^{\infty} \tilde{r}_k (G(\tilde{r}_k) + G(\tilde{r}_{k-1})) + \text{const.} \end{aligned} \quad (11)$$

where we have defined $r_0 = 0$, $\tilde{r}_i = r_i + \ell^*/2$, and $G(r) = \int_r^{\infty} dr' p(r')$. Note that the agent finds the source instantly if $r^* < \ell^*/2$.

In the absence of the constraint $\tilde{r}_{k+1} - \tilde{r}_k \leq \ell^*$, this problem has exactly the same objective (up to an irrelevant affine transformation) as the linear search problem (LSP) [11–14]. It is therefore useful to study solutions of the LSP. We have

$$\frac{1}{\pi} \frac{\partial J}{\partial \tilde{r}_i} = G(\tilde{r}_i) + G(\tilde{r}_{i-1}) - p(\tilde{r}_i)(\tilde{r}_i + \tilde{r}_{i+1}) \quad (12)$$

where $G(r) = \int_r^{\infty} dr' p(r')$. Therefore, in the absence of the constraint, an optimal choice of the \tilde{r}_k must satisfy $\partial J / \partial \tilde{r}_i = 0$, whence we have the recurrence

$$\tilde{r}_i + \tilde{r}_{i-1} = \frac{G(\tilde{r}_i) + G(\tilde{r}_{i-1})}{p(\tilde{r}_i)}. \quad (13)$$

B. Sufficient condition for saturation of Eq. 10

The critical question is, for what distributions $p(r)$ do the optimal \tilde{r}_k satisfy

$$\tilde{r}_{k+1} - \tilde{r}_k \geq \ell^*$$

for sufficiently large k in the unconstrained problem? This leads to $\tilde{r}_{k+1} - \tilde{r}_k = \ell^*$ upon reintroducing the constraint, which in turn leads to diffusive scaling (see below).

While we do not attempt to answer this question completely, it is possible to show that probability densities which decay exponentially or slower eventually satisfy this inequality. The sketch of the proof is as follows: first, it is straightforward to show that, for any sufficiently well-behaved probability density $p(r)$ on $(0, \infty)$ with finite mean and

$p(r) > 0$ everywhere,

$$p(r)^{-1} \int_r^\infty dt p(t) \leq Cr, \quad (14)$$

for some $C \in (0, 1)$ and for sufficiently large r . This follows after application of L'Hôpital's rule to the expression $\int_r^\infty dt p(t)/rp(r)$.

We now assume $p(r)$ decays exponentially or slower—that is, suppose that if $x > 0$,

$$p(r+x)/p(r) \geq \exp(-x/a) \quad (15)$$

for large enough r . Then using the recursion Eq. 13 and Eq. 14,

$$\begin{aligned} 2\tilde{r}_k &\leq \tilde{r}_k + \tilde{r}_{k+1} \\ &= 2p(\tilde{r}_k)^{-1} \int_{\tilde{r}_k}^\infty dr p(r) + \int_{\tilde{r}_{k-1}}^{\tilde{r}_k} dr \frac{p(r)}{p(\tilde{r}_k)} \\ &\leq 2C\tilde{r}_k + \int_{\tilde{r}_{k-1}}^{\tilde{r}_k} dr e^{(\tilde{r}_k-r)/a} \\ &= 2C\tilde{r}_k + a \left(e^{(\tilde{r}_k-\tilde{r}_{k-1})/a} - 1 \right). \end{aligned}$$

Rearranging, we have

$$\tilde{r}_k - \tilde{r}_{k-1} \geq a \log \left(\frac{2(1-C)\tilde{r}_k}{a} + 1 \right). \quad (16)$$

The RHS grows without bound, since the optimal \tilde{r}_k are themselves increasing and unbounded. Therefore, in the absence of the constraint, $\tilde{r}_k - \tilde{r}_{k-1} \geq \ell^*$ for large enough k .

For our olfactory search problem, for large U , the correct $p(r)$ to consider is $p(r) = x_0^{-1} \exp(-r/x_0)$ (see Eq. 9). Equation 15 then holds trivially, and we can conclude that, indeed, $\tilde{r}_{k+1} - \tilde{r}_k = \ell^*$ asymptotically. The result also holds e.g. for power laws $p(r) \propto r^{-\alpha}$ for $\alpha > 2$.

C. Linear growth of the \tilde{r}_k leads to diffusive scaling

Having established that $\tilde{r}_{k+1} - \tilde{r}_k = \ell^*$ for large enough k , it is easy to see that $t^{1/2}$ scaling follows inevitably. We have

$$\dot{r} = r'(\theta)\dot{\theta} \simeq \ell^* \frac{v}{r},$$

whence $r(t) \simeq \sqrt{2\ell^*vt}$, and

$$\dot{\theta} \simeq \frac{v}{r} \simeq \sqrt{\frac{v}{2\ell^*t}}$$

whence $\theta(t) \simeq \sqrt{\frac{2vt}{\ell^*}}$. Together, these expressions for $r(t)$ and $\theta(t)$ describe an Archimedean spiral with asymptotically constant speed. Adapting them to the cone easily yields Eq. 5 from the main text.

As an aside, Archimedean spirals are observed both in the present work and previous studies, so it is tempting to apply the same simplified low-information model (Eq. 4 in the main text) to the isotropic problem. However, the isotropic problem lacks a substantial region where $p_1 \simeq 1$, so the model's validity is dubious and we cannot determine the characteristic lengthscale of the spiral with such an argument.

D. A family of fast-decaying distributions which lead to subdiffusive scaling

It is also interesting to try to understand when Eq. 10 is *not* asymptotically saturated. Intuitively, if $p(r)$ decays sufficiently quickly, the extra time it takes to sweep out circles with larger radii will outweigh the benefit of sweeping

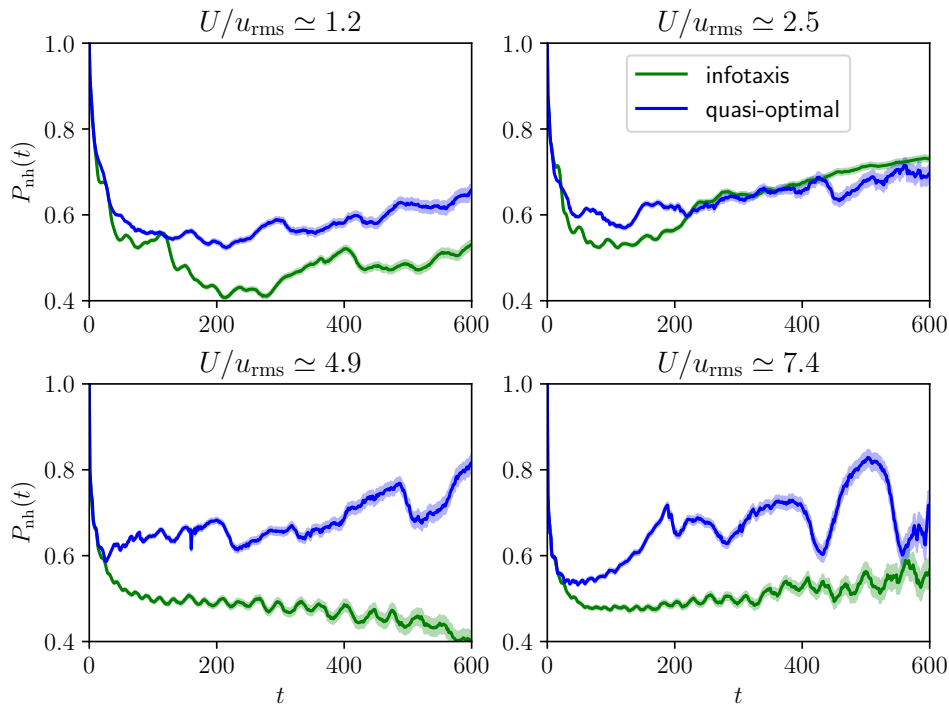


FIG. 4:

out more probability mass per unit time, so the agent will be incentivized to move outward very slowly.

Again, we do not attempt to answer this question in full generality. However, in particular, one can show that compressed exponentials of the form $p(r) \propto \exp(-r^\beta)$ for $\beta > 1$ have optimal $\tilde{r}_{k+1} - \tilde{r}_k$ tending toward 0. We suppress details since the result is a straightforward generalization of Lemmas 4.1–4.3 from Ref. [12], which studied the special case of a Gaussian distribution $p(r) \propto \exp(-r^2/2)$.

The upshot is that if $p(r)$ decays faster than exponential, Eq. 10 will *not* be asymptotically saturated by an optimal policy, at least for one family of distributions which includes Gaussians. This, in turn, will lead to scaling in time slower than $r \sim t^{1/2}$. (N.B., if $p(r)$ decays too quickly, then we risk breaking the approximation that allowed us to consider a prior supported only on a cone.)

$P_{\text{nh}}(t)$, as defined in the main text, is shown for all wind speeds in Figs. 4–5. The mean squared displacement (MSD) data are presented in Figs. 6–7. In the isotropic case, we also show the mean squared polar angle $\langle \theta(t) \rangle$. As a reminder, an ensemble of 10^4 trajectories for each wind speed was used to estimate the

E.

Also included in the Supplemental Material as separate files are movies, in .gif format, of no-hit trajectories at all wind speeds, for both infotaxis and quasi-optimal trajectories. The beginning of the file name indicates the first digit of the normalized wind speed.

-
- [1] A. Loisy and C. Eloy, Searching for a source without gradients: how good is infotaxis and how to beat it, *Proceedings of the Royal Society A* **478**, 20220118 (2022).
 - [2] R. A. Heinonen, L. Biferale, A. Celani, and M. Vergassola, Optimal policies for Bayesian olfactory search in turbulent flows, *Physical Review E* **107**, 055105 (2023).
 - [3] A. Loisy and R. A. Heinonen, Deep reinforcement learning for the olfactory search POMDP: a quantitative benchmark, *The European Physical Journal E* **46**, 17 (2023).
 - [4] H. Kurniawati, D. Hsu, and W. S. Lee, Sarsop: Efficient point-based POMDP planning by approximating optimally reachable belief spaces., in *Robotics: Science and systems*, Vol. 2008 (Citeseer, 2008).

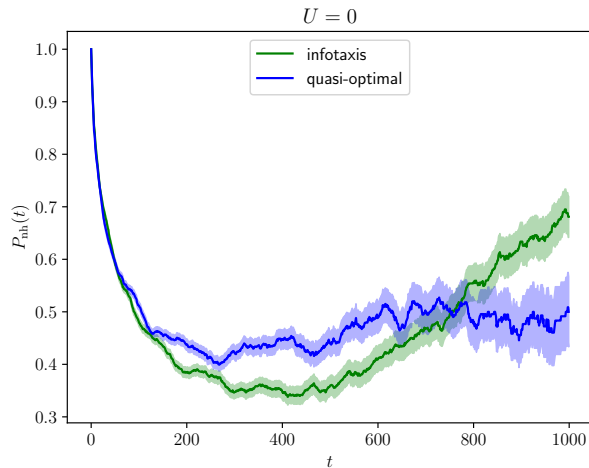
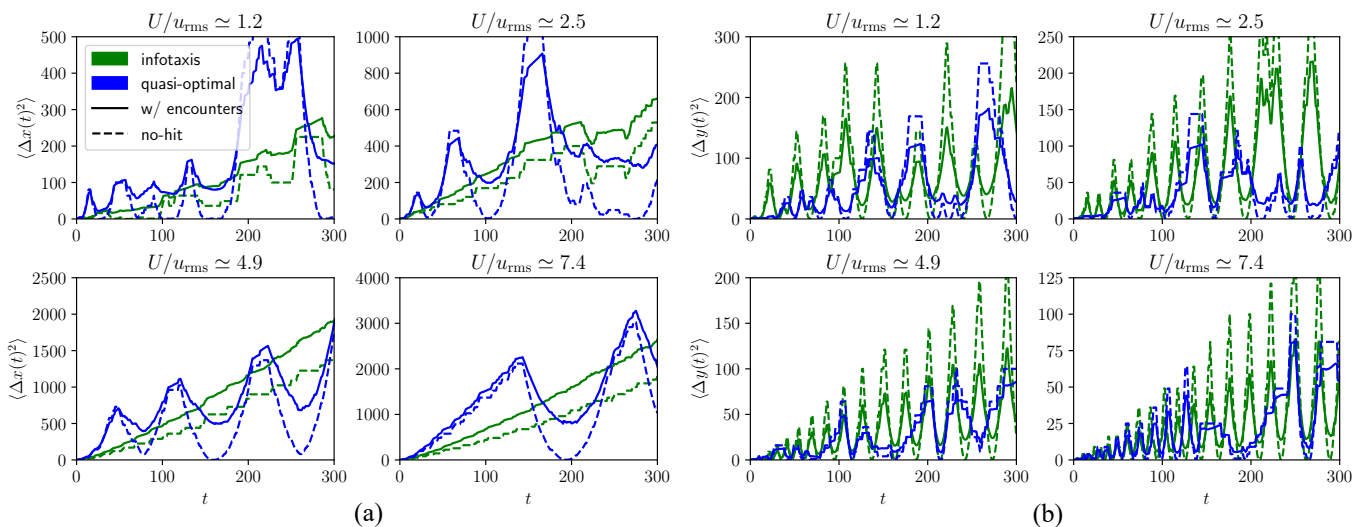


FIG. 5:

FIG. 6: Mean squared displacements in \hat{x} and \hat{y} directions, for all nonzero wind speeds, taken from ensembles of 10^4 trajectories and compared to the squared displacement in the no-hit trajectory (dashed lines).

- [5] E. J. Sondik, The optimal control of partially observable markov processes over the infinite horizon: Discounted costs, *Operations research* **26**, 282 (1978).
- [6] L. P. Kaelbling, M. L. Littman, and A. R. Cassandra, Planning and acting in partially observable stochastic domains, *Artificial intelligence* **101**, 99 (1998).
- [7] G. Shani, J. Pineau, and R. Kaplow, A survey of point-based POMDP solvers, *Autonomous Agents and Multi-Agent Systems* **27**, 1 (2013).
- [8] M. T. Spaan and N. Vlassis, Perseus: Randomized point-based value iteration for POMDPs, *Journal of artificial intelligence research* **24**, 195 (2005).
- [9] B. I. Shraiman and E. D. Siggia, Scalar turbulence, *Nature* **405**, 639 (2000).
- [10] A. Celani, E. Villermaux, and M. Vergassola, Odor landscapes in turbulent environments, *Physical Review X* **4**, 041015 (2014).
- [11] A. Beck, On the linear search problem, *Israel Journal of Mathematics* **2**, 221 (1964).
- [12] A. Beck and M. Beck, Son of the linear search problem, *Israel Journal of Mathematics* **48**, 109 (1984).
- [13] A. Beck and M. Beck, The linear search problem rides again, *Israel Journal of Mathematics* **53**, 365 (1986).
- [14] S. Alpern and S. Gal, *The theory of search games and rendezvous*, International Series in Operations Research & Management Science, Vol. 55 (Springer Science & Business Media, 2003).

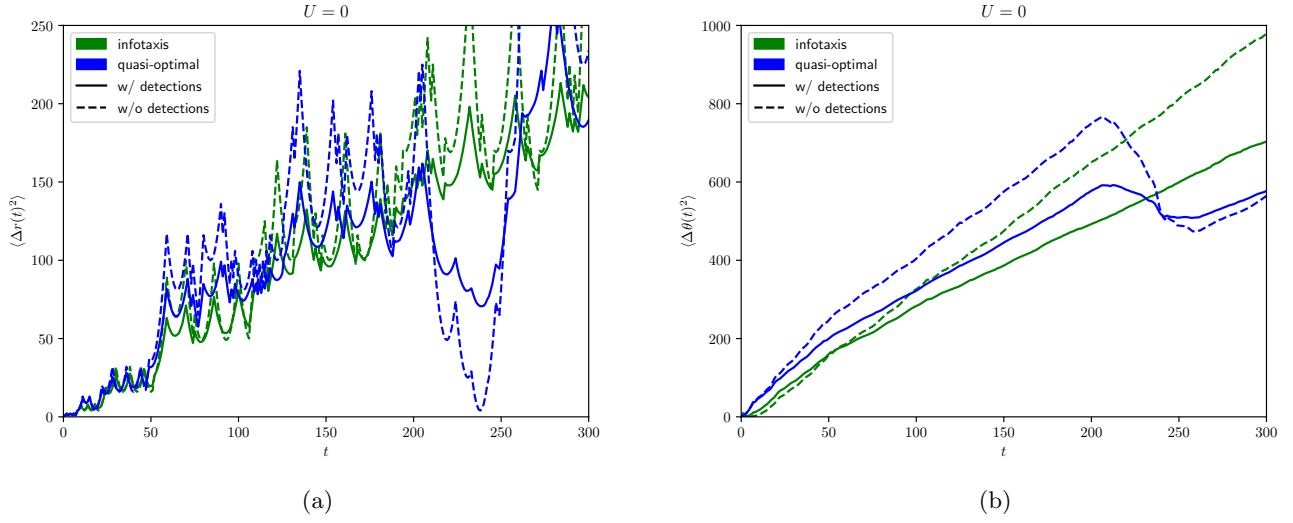


FIG. 7: (a) The mean squared displacement $\langle r(t)^2 \rangle = \langle x(t)^2 + y(t)^2 \rangle$ and (b) the mean squared polar angle $\langle \theta(t)^2 \rangle$ in the isotropic problem, taken from an ensemble of 10^4 trajectories. The results are roughly consistent with $r \propto t^{1/2}$ and $\theta \propto t^{1/2}$, which describes an Archimedean spiral.

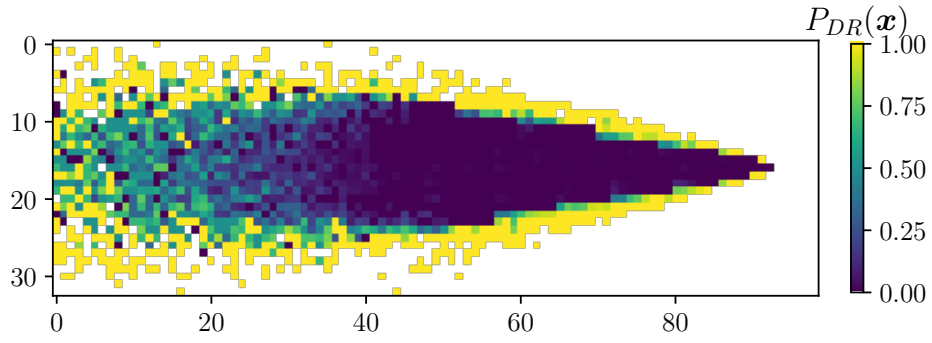


FIG. 8:

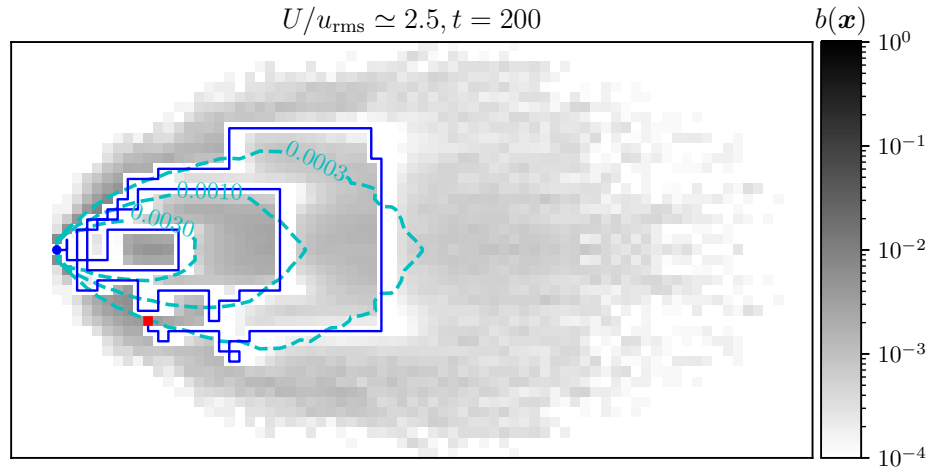


FIG. 9:

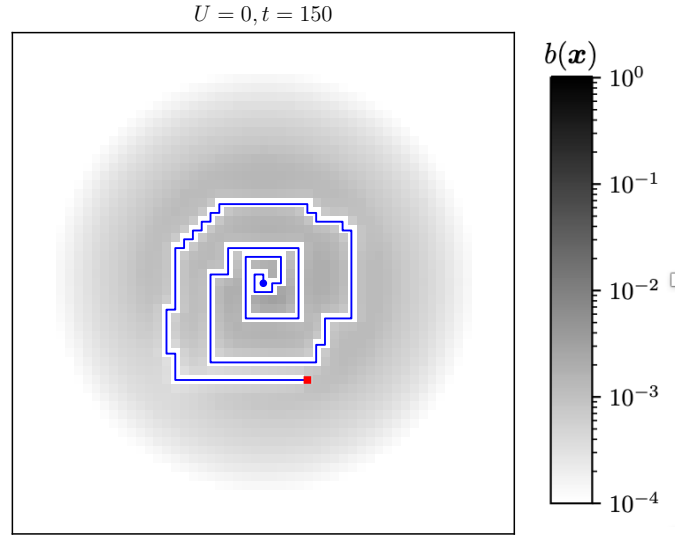


FIG. 10:

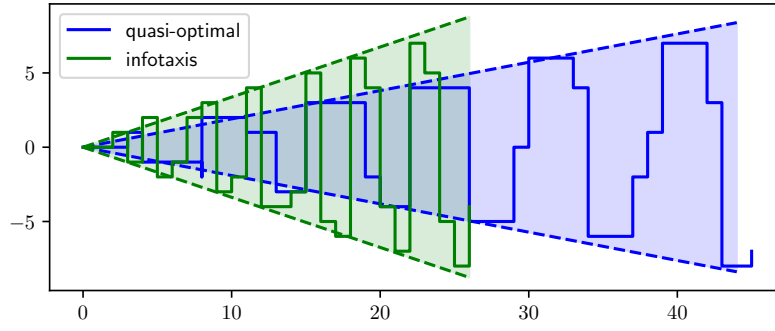


FIG. 11: Quasi-optimal and infotactic no-hit trajectories for $U/u_{\text{rms}} \simeq 7.4$, along with a best fit to the cones of exploration, which have been outlined with dashed lines and shaded. The trajectories are shown at $t_R = 150$, the starting point for the quasi-optimal policy's downwind return.